ABSOLUTE CALIBRATION OF AVHRR CHANNELS 1 AND 2

E. VERMOTE AND NAZMI EL SALEOUS
NASA / Goddard Space Flight Center,
Greenbelt, MD, 20771,
U.S.A.

Abstract. This chapter considers the calibration of channels 1 and 2 of the Advanced Very High Resolution Radiometers (AVHRR), a crucial process for the quantitative interpretation of remotely sensed data acquired through time. In this chapter, a new method of absolute calibration of the first two AVHRR channels based on observation of oceans and deep thick clouds is presented, along with sensitivity tests on the possible error sources. Calibration results obtained by this method for NOAA- 7, -9 and -11 from 1981 to the present are also included, as is a comparison of the derived NOAA-9 values with other recently published ones.

1. Introduction

As was shown in the previous chapter, separating the atmospheric and ground signals in Advanced Very High Resolution Radiometer (AVHRR) data is an important step towards the use of these data in quantitative studies. This chapter deals with a related issue, radiometric calibration. The AVHRR data, in common with those from other Earth observation satellite sensors, are originally recorded as digital counts or numbers (DNs). These may be converted to radiance values through the use of appropriate calibration coefficients. These coefficients (gain and offset) are usually supplied from pre-flight calibration of the sensor. However, large changes can, and do, occur to the optical system, both during and post-launch. Onboard calibration devices are designed to take these into account, but unfortunately no such devices are available for the AVHRR visible and near-infrared sensors. Thus, comparison of data from different AVHRR sensors, or time-series from a single sensor, should ideally incorporate the use of absolute calibration coefficients which take into account the post-launch changes in sensor performance.

Several methods, both relative and absolute, have been developed for this purpose over both land and ocean surfaces (Frouin and Gautier 1987, Smith *et al.* 1988, Whitlock *et al.* 1988, Holben *et al.* 1990, Staylor 1990, Teillet *et al.* 1990, Brest and Rossow 1991, Abel *et al.* 1993, Kaufman and Holben 1993). Relative calibration methods do show relative sensor degradation but they also need to be related to some absolute value. Aircraft calibration (*e.g.* as carried out by Abel *et al.* 1993) is expensive and cannot be applied to historical datasets. Other absolute calibration methods combining surface and atmospheric ground-based measurements (Teillet *et al.* 1990) suffer from problems in sampling of the surface and uncertainty in accounting for bidirectional relectance distribution function (BRDF) effects.

This chapter describes a recent and robust method for absolute sensor calibration based on the approach of Kaufman and Holben (1993). This method, first introduced by

G. D'Souza et al. (eds.), Advances in the Use of NOAA AVHRR Data for Land Applications, 73–92.

Vermote *et al.* (1992) for the calibration of the SPOT/HRV radiometer, unlike previous methods, takes into account the actual precipitable water vapour and aerosol optical thickness qualities of the atmosphere at the time of imaging.

2. Sensor calibration

Ocean areas have often been used to calibrate satellite sensors. For example, Koepke (1982) used ground and atmospheric measurements to calibrate the METEOSAT sensor and Fraser and Kaufman (1986) developed a method for the calibration of the Visible Infrared Spin Scan Radiometer (VISSR with effective wavelength of 0.61 μm), carried onboard GOES-5 and 6. The latter method concerned the relating of the observed digital count to the actual reflectance by assuming mean conditions both for the atmosphere and the ocean - the dominant signal being modelled for areas outside the ocean glint pattern. This method was then adapted also to calibrate AVHRR channel 1 (Kaufman and Holben 1993).

In this chapter we report on developments of the Kaufman and Holben (1993) approach. Correction of channel 2 is introduced, and channel 1 and 2 intercalibration used to reduce the uncertainty due to variability in surface and atmospheric conditions, which relate principally to wind speed and aerosol concentration respectively. The theoretical background and accuracy of this method is described and examined, and the method is then applied to the AVHRR sensors on NOAA-7, -9 and -11, from 1981 to the present. Split-window water vapour estimates form part of the output of this method, and these are then validated by ancillary data from the SSMI sensor. Finally, the results obtained for NOAA-9 are validated by comparison with other recently published values.

3. Intercalibration between channel 1 and 2

3.1. METHOD

The method of calibration described in this chapter is based on AVHRR observations of high clouds. These may be considered lambertian reflectors and, if they are sufficiently thick, the effects of the atmosphere and surface below them can be ignored. Therefore, the signal at the top of the atmosphere can be written as a function of the cloud top altitude z:

$$\rho^*(z) = T_g \left[\rho_a(z) + T_a \frac{\rho_{cloud}}{1 - S(z)\rho_{cloud}}\right] \quad (1)$$

where Tg represents the gaseous transmission, $\rho_a(z)$ is the intrinsic reflectance of the atmosphere above the cloud, $T_a(z)$ is the transmission of the atmosphere above the cloud, and S(z) is the albedo of the atmosphere above the cloud.

If the cloud is high enough (above 4 km), then the aerosol and water vapour influence on the signal can also be ignored because these are normally present only in the lower

layers of the atmosphere. Therefore, the signal could be written for both channels 1 and 2 of the AVHRR as:

$$\rho_1 = Tg_{oz1}\, Tg_{ox1} \left[\rho_{r1}(z) + T_{r1}(z) \quad \frac{\rho_{cloud}}{1 - S_{r1}(z)\rho_{cloud}}\right] \tag{2a}$$

$$\rho_2 = Tg_{oz2}\, Tg_{ox2} \left[\rho_{r2}(z) + T_{r2}(z) \quad \frac{\rho_{cloud}}{1 - S_{r2}(z)\rho_{cloud}}\right] \tag{2b}$$

In practice we have:

$$\rho_{m1} = \rho_1 r_1 = Tg_{oz1}\, Tg_{ox1} \left[\rho_{r1}(z) + T_{r1}(z) \quad \frac{\rho_{cloud}}{1 - S_{r1}(z)\rho_{cloud}}\right] r_1 \tag{3a}$$

$$\rho_{m2} = \rho_2 r_2 = Tg_{oz2}\, Tg_{ox2} \left[\rho_{r2}(z) + T_{r2}(z) \quad \frac{\rho_{cloud}}{1 - S_{r2}(z)\rho_{cloud}}\right] r_2 \tag{3b}$$

where ρ_{m1}, ρ_{m2} are the measured AVHRR signals with pre-flight calibration for channels 1 and 2 (Price 1987, Price 1988) and r_1 and r_2 are the respective degradation coefficients (Kaufman and Holben 1993).

Therefore, assuming $\rho_r(z)\, r \cong \rho_r(z)$, it can be shown that:

$$\rho'_1 = \frac{\dfrac{\rho_{m1}}{Tg_{oz1} Tg_{ox1}} - \rho_{r1}(z)}{T_{r1}(z)} \tag{4a}$$

$$\rho'_2 = \frac{\dfrac{\rho_{m2}}{Tg_{oz2} Tg_{ox2}} - \rho_{r2}(z)}{T_{r2}(z)} \tag{4b}$$

where ρ'_1 and ρ'_2 are the corrected signals for molecular scattering and gaseous absorption. Then, correcting for the atmospheric albedo, $S_r(z)$, it can be shown that:

$$\rho''_1 = \frac{\rho'_1}{1 + S_{r1}(z)\rho'_1} \cong r_1\, \rho_{clouds} \tag{5a}$$

$$\rho''_2 = \frac{\rho'_2}{1 + S_{r2}(z)\rho'_2} \cong r_2\, \rho_{clouds} \tag{5b}$$

So, $\rho''_1/\rho''_2 = r_1/r_2 = r_{12}$ assuming that the cloud reflectance is constant for all wavelengths in the region of 0.60 to 1.0 μm.

3.2. ERROR BUDGET

3.2.1 *Lambertian Clouds.* In order to minimise the gaseous absorption and scattering effects, the clouds chosen for use in this method are restricted to those within angles of view of between 0 and 10 degrees. Furthermore, because it is the ratio of cloud reflectances that is utilised, any remaining errors resulting from the assumption of lambertian behaviour are expected to cancel out.

3.2.2. *Aerosol and Water Vapour.* Clouds are chosen relative to their apparent brightness temperature in AVHRR Channel 4 in the range from 220 K to 225 K at tropical latitudes. This corresponds to an altitude range of 8 km to 13 km, which is well above the layers at which water vapour or aerosols are present. Figure 1 shows the variation of the signal observed over clouds for both channels versus the temperature in channel 4 (10.8 μm). Both channel 1 and 2 signals increase when the temperature decreases due to the decreasing amount of water vapour and other molecules above the cloud. Figure 2 shows the calibration ratio, r_1/r_2, versus temperature. The clouds selected to determine the ratio are located at the lower end of the temperature range where the water vapour effect is minimal and the ratio therefore reaches a plateau. By running a gaseous aborption model, it can be shown that the residual absorption by water vapour at this range of altitude is only of the order of 2-3% (in channel 2) depending on the atmospheric profile. Since our clouds are also situated in the moist tropical convective zone it was consequently felt appropriate to adopt a general correction factor of 0.97.

3.2.3. *Rayleigh Correction.* For clouds of apparent reflectance greater than 0.5 and higher than 8 km, for view zenith angle lower than 30°, the terms ρ_r, T_r and S_r only influence about 1% of the total signal. Therefore, using pre-flight calibration coefficients to correct for Rayleigh scatter, this will lead to a subsequent error of only 0.3%.

3.2.4. *Ozone and Oxygen Correction.* The overall amount of oxygen absorption is weak in both channels and depends mainly on altitude. As the uncertainty regarding cloud altitude should be less than 1 km, so the uncertainty concerning total oxygen amount should be less than 5%. Thus, the variation of the transmission in channels 1 and 2 due to the variation of oxygen amount is negligible.

The corrections used for ozone absorption are based on the ozone amounts taken from the latitudinal monthly climatological data published by London *et al.* (1976). The relative accuracy of these included ozone amounts should be in the order of 10%, which translates, for an airmass of 2, to an uncertainty of only 1.0% in the radiance for channel 1, and therefore to a similarly low uncertainty value for the ratio r_{12}.

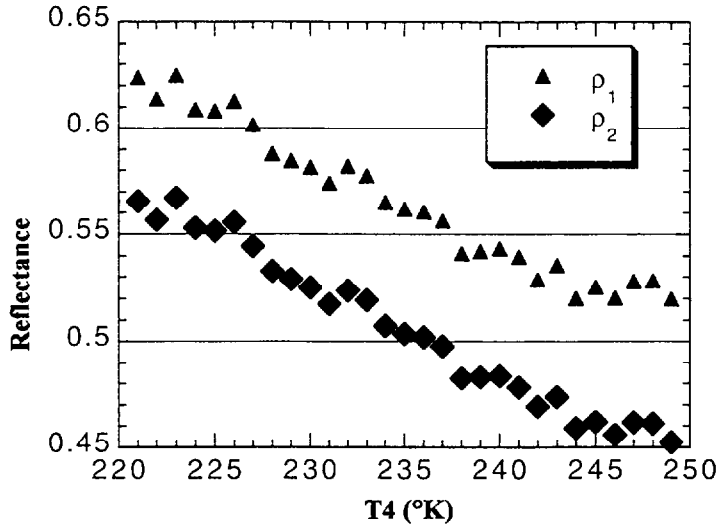

Figure 1. Cloud reflectances observed in channel 1 and 2 of the AVHRR as a function of T4.

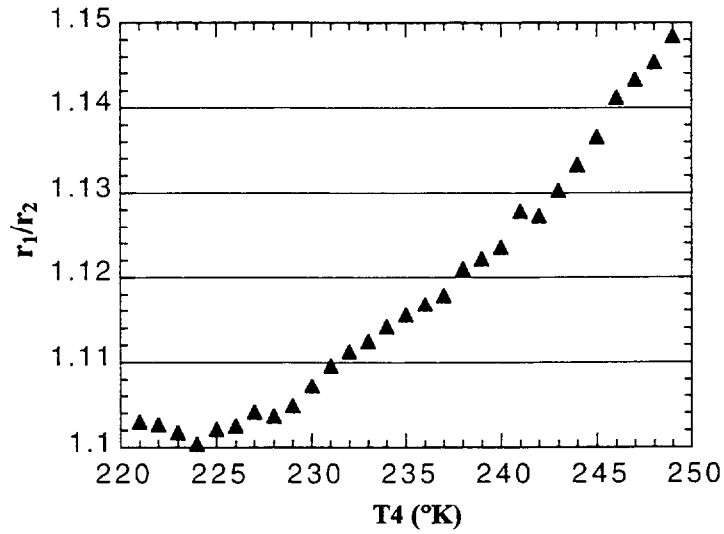

Figure 2. The ratio r_1/r_2 as a function of the temperature in channel 4.

3.2.5. *Total Error.* If we sum (in quadratic) all the error sources listed above, the overall uncertainty of the method is only about 2%. Other sources of error can probably be kept to a minimum. For example, the errors due to stratospheric aerosol effects can be minimised by avoiding the areas of the highest concentrations of aerosols as depicted by operational aerosol monitoring datasets, such as the NOAA weekly composite (Stowe *et al.* 1992) or SAGE data sets (McCormick and Veiga 1992). The main assumption on which the success of the method is dependent is that cloud reflectance does not vary much between the visible and near-infrared windows. This hypothesis is problably true for high thick clouds, which are not influenced by tropospheric aerosol in the way they form. The analysis of long-term continuous datasets, as we will demonstrate in the next section, is one way of verifying the error budget because the error sources themselves will probably be far more variable in time than sensor deterioration.

4. Rayleigh calibration for Channel 1

4.1. METHOD

For a cloudless air mass over the ocean with only a small amount of haze and a reasonable distance from regions of sun glint, the major contribution to the upward radiance in the visible part of the spectrum is from molecular scattering (in the order of 70-80 %). This amount can be accurately computed from a radiative transfer model (Deuzé *et al.* 1989) and can then be used for sensor calibration (Fraser and Kaufman 1986, Kaufman and Holben 1993, Vermote *et al.* 1991). Theoretical signals may then be computed in both channels assuming, for example, a chlorophyll content of 0.3 mg/l and a wind speed of 10 ms^{-1}, for several water vapour values, and an aerosol model representative of maritime-aerosol particle distribution with optical thickness from 0.10 at 0.55 μm (Deuzé *et al.* 1989). In our case, the absorption effect of ozone and oxygen was computed using an explicit formulation (Tanré *et al.* 1992) fitted from running the 5-S radiative transfer code (see the previous chapter and Tanré *et al.* 1990).

The degradation calibration coefficient r_1 is defined by:

$$r_1 = \frac{\rho_1^m}{\rho_1^r} \tag{6}$$

where ρ_1^m is the radiance measured by the sensor using the pre-flight calibration and ρ_1^r is the real radiance.

Since the amount of aerosol and/or wind speed is different from those used in the theoretical computations, the theoretical radiance, ρ^t has to be corrected by an offset $\delta\rho_1$

$$\rho_1^r = \rho_1^t + \delta\rho_1 \tag{7}$$

At satellite level this equation then becomes:

$$\rho_1^m = r_1 \rho_1^t + r_1 \delta\rho_1 \quad (8)$$

A discrepancy will also be observed in channel 2, that is:

$$\rho_2^m \; r_2 \rho_2^t + r_2 \delta\rho_2 \quad (9)$$

where $\delta\rho_1$ is related to $\delta\rho_2$ through the spectral dependence of this perturbation I_{12}:

$$\delta\rho_1 = I_{12}\delta\rho_2 \quad (10)$$

I_{12} is derived from simulations of the signal for both channels 1 and 2 with an aerosol optical thickness of 0.15 and 0.05.

Therefore, ρ_1^m may be written as :

$$\rho_1^m = r_1 \rho_1^t + r_1 I_{12} (\rho_2^m - r_2 \rho_2^t) / r_2 \quad (11)$$

and, solving for r_1 it was found that:

$$r_1 = \frac{\rho_1^m - r_{12} I_{12} \rho_2^m}{\rho_1^t - I_{12} \rho_2^t} \quad (12)$$

where r_{12} is the intercalibration coefficient computed with the method previously outlined and is equal to r_1/r_2.

In practice, the calculation of r_1 is based on more than one measurement. The data are extracted from the Pacific Ocean data set referred to above. For a period of nine days, rigourous cloud screening is performed using the methods of Stowe *et al.* (1991). Then, a composite of the non-cloudy pixels and non-cloud-shadowed pixels is produced using the minimum value in channel 1. The result of this "geometrical composite" is then screened manually to select a zone of 25 scans where the cloud amount is low and the Rayleigh contribution significant (in practice as close to the principal plane as possible). An average value for non-cloudy pixels is then calculated for each view direction for both channels. The values, after subtracting the deep-space count, are then converted to reflectance units using the pre-flight calibration coefficient (Figure 3). For each pixel of the anti-specular portion of the scan (angle of view between 40-70 degrees) the numerator of Equation (12) is shown plotted against the denominator of the same Equation 12 (Figure 4) (with the water vapour amount as given by the split window technique) (Vermote *et al.* 1993). Then the slope of the linear regression of the numerator (measured reflectance) versus the denominator (predicted reflectance) is the degradation coefficient r_1. Both the intercept (which should be small) and the correlation coefficient (which should be high) provide good indicators of the accuracy of the calibration.

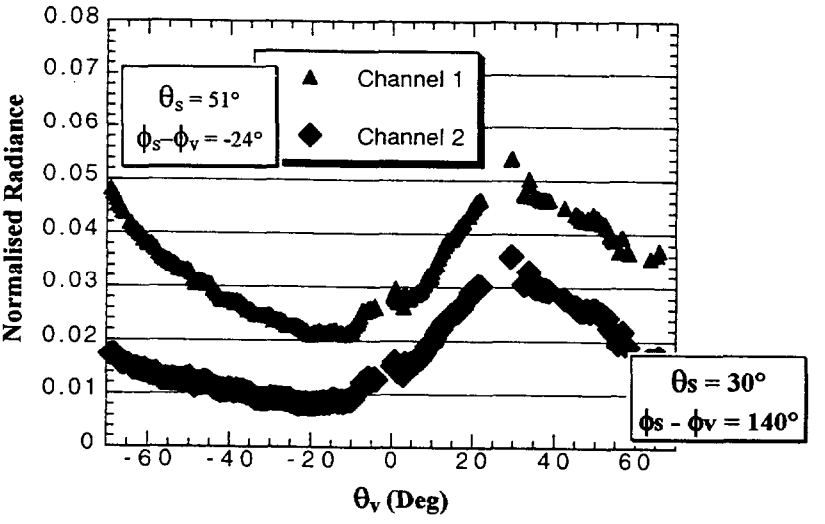

Figure 3. Radiances observed in channel 1 and 2 of the AVHRR over ocean.

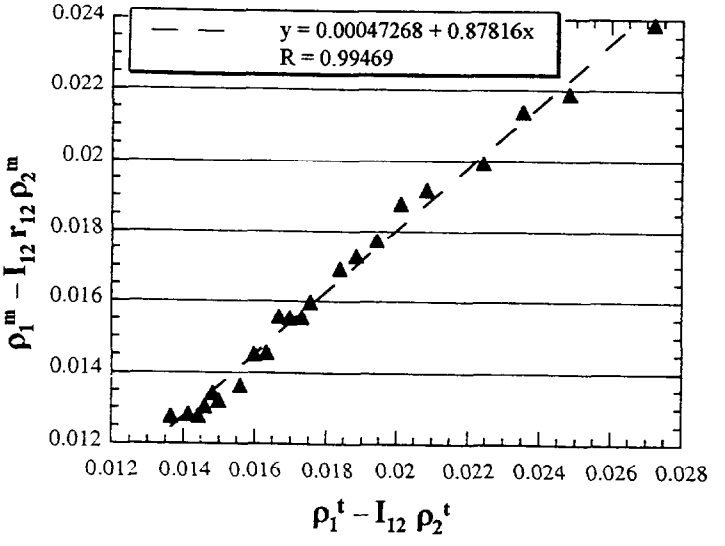

Figure 4. Linear regression between the numerator of Equation 12 *(y)* and the demoninator of Equation 12 *(x)*, that leads to an estimate of degradation (r_1), the slope of the linear regression.

4.2. ERROR BUDGET

Even after we assume perfect linearity for the instrument, and stability in the spectral response, several other sources of uncertainty remain. Basically, these are uncertainties in the radiative computation of the model, and errors in: input parameters for ozone and water vapour amount, ocean colour, pressure and, finally, errors in the estimation of I_{12} because of an assumed aerosol type and constant wind speed. The relative magnitude of these error sources is further discussed below.

4.2.1. *Intercalibration Coefficient (r_{12}).* The error on r_{12} estimated at 2% will be directly related to r_1 (Equation 12) as described above (section 3.2.4).

4.2.2. *Radiative Transfer Computation.* If the sun is never lower than 75° over the horizon, the accuracy of the radiative transfer calculation based on plane parallel approximation is better than $1x10^{-3}$ in reflectance units (Vermote and Tanré 1992). Thus for the given level of radiance ($2x10^{-2}$) and sun angle (75°), of the pixels we are using for calibration, there will be a relative uncertainty due to the radiative transfer computation in the order of only 1%.

4.2.3. *Gaseous Absorbers.* The ozone amount used in the computation, which primarily affects the signal in channel 1, is the latitudinal monthly climatological data (London *et al.* 1976). The assumed relative accuracy of the ozone amount should be of the order of 10%. That translates, for an airmass of 4, to an uncertainty of only 1.5% in the radiance for channel 1. This uncertainty is translated to an uncertainty of 2% for the calibration coefficient (see Equation 12), as a typical ratio from channel 1 to channel 2 over clear water is 2.

The expected accuracy in the determination of the total column water vapour amount is 0.5 cm. Water vapour is mainly distributed in the lower layer of the atmosphere (0-2 km) and most of the water vapour absorption occurs in the longer spectral wavelength region of channel 2. Therefore, uncertainty in the determination of the total column water vapour amount will translate directly to an uncertainty in the aerosol correction process. The radiation transfer code 5S was again used to determine the amount of possible uncertainty on transmission; this was found to be in the order of 2%. For a typically clear day with an aerosol amount of 0.1 m this translates to a residual of $2x10^{-4}$ in reflectance units (assuming that 0.1 m gives 0.01 reflectance units). That leads to an uncertainty of only 0.1% in r_1 for a typical value of the numerator of Equation 12.

4.2.4. Ocean Colour. The effect of ocean colour was determined using data from an area over the Pacific Ocean well away from the coast to avoid turbidity effects. According to data from the Coastal Zone Color Scanner (CZCS), if the chlorophyll content is lower than 0.3 mg/l and known with an accuracy better than 0.1 mg/l, this would lead to an uncertainty of only $1x10^{-4}$ in reflectance units for channel 1, which translates to an uncertainty of only 0.1% for the calibration coefficient.

4.2.5. *Pressure.* The data set used in this study was completely free of clouds, typical of a high-pressure weather system, and a pressure of 1010 millibars (Mb) was consequently assumed. If the pressure is known to within an accuracy of 10 millibars (Mb), then the Rayleigh optical thickness can be determined to within 1% in both channels. This would lead to an uncertainty of only 1% for the calibration coefficient.

4.2.6. *Wind Speed.* A simulation was performed in order to assess the uncertainty induced by wind speed. The wind speed was taken as 10 m/s and a simulation of the measured radiance was made at 5 m/s and 15 m/s with all the other parameters remaining fixed (Pressure = 1010 Mb, maritime aerosol model, aerosol optical thickness = 0.1). The wind speed affects the signal at the top of the atmosphere in two ways: on the sun glint by changing the distribution of wave slopes (Cox and Munk 1965) and by changing the area covered by foam (Koepke 1984). The latter is the most important effect because the calibration is done in the backscattering direction where the direct sunglint influence is low.

Figure 5 gives the values observed in channel 1 and 2 for the nomimal wind speed as well as at 5 m/s and 15 m/s. It also gives the values of the calibration coefficient (equal to 1 for the nominal wind speed). It can be deduced that the effect of wind speed introduces a relative uncertainty of about 2%.

4.2.7. *Aerosol Type.* A simulation was performed for two aerosol types in addition to the maritime model: for continental aerosol at an optical thickness of 0.1 and 0.25 and for stratospheric aerosol (King *et al.* 1984) at optical thicknesses of 0.1, 0.2 and 0.3. In each case, the error is significant, ranging from 5% to 15%. We do not expect continental aerosol to be present all the time over the ocean, especially after the compositing process used. In cases where stratospheric aerosol concentration is significant, for example following the Pinatubo or El Chichon volcanic eruptions, the method presented is not expected to work, at least in its current state. In the total error budget, any uncertainty due to aerosol type is not reported. This assumes that there is no stratospheric aerosol contamination, that the composite eliminates continental aerosol outbreaks, and also that the haze is perfectly representative of the mean aerosol background over the Pacific Ocean.

4.2.8. *Total Error.* Adding all the effects listed above, the theoretical error budget shows that, under reasonable aerosol loading, the intercalibration coefficient can be determined to within a precision of 4%. This figure relies largely on the fact that strong aerosol contamination is avoided. Any dubious results could be filtered out by inspecting the correlation and intercept of the regression (see Figure 4). The consistency of the result over a month (four weekly results) should also confirm the estimate and the size of its likely error.

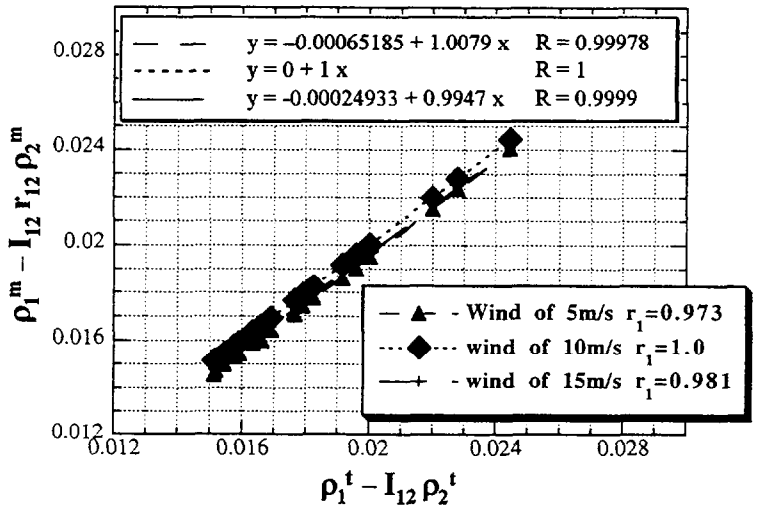

Figure 5. Effect of wind speed on the determination of r_1.

5. Calibration results

Figure 6 shows intercalibration coefficient estimates for NOAA-7, -9 and -11 obtained using the cloud technique. The spread of values is very low (less than 2%).

Figure 7 shows the estimate of the degradation in channel 1, using the ocean technique. Points where the intercept was found to be larger than $2x10^{-3}$ were eliminated. The results were also averaged over a period of 36 days (four composites) to minimise noise. Once again, the results are very encouraging; the stability of the derived coefficient, 4-5%, is inside our error budget estimate. There is a seasonal variation of about ±2% which can be attributed to the ozone variability. The data are actually reprocessed to address that point.

Figure 8a shows the comparison between U2 aircraft calibration (Abel *et al.* 1993) and our result from the cloud calibration method for NOAA-9. Figure 8b shows the same comparison for NOAA-11. The temporal trends from both methods, and even the absolute values, agree reasonably well. The figures also show values from Che and Price (1992) obtained from a compilation of various previously published methods.

For the Ocean method, Figures 9a-b show comparisons for both NOAA-9 and NOAA-11 respectively between U2 estimates and our results. In both cases, the value for deterioration observed over the ocean is well below the value determined by the U2 or others. However, this degradation has also been reported for NOAA-11 by Mitchell *et al.* (1992). The values from their paper are also plotted on the figure for comparison.

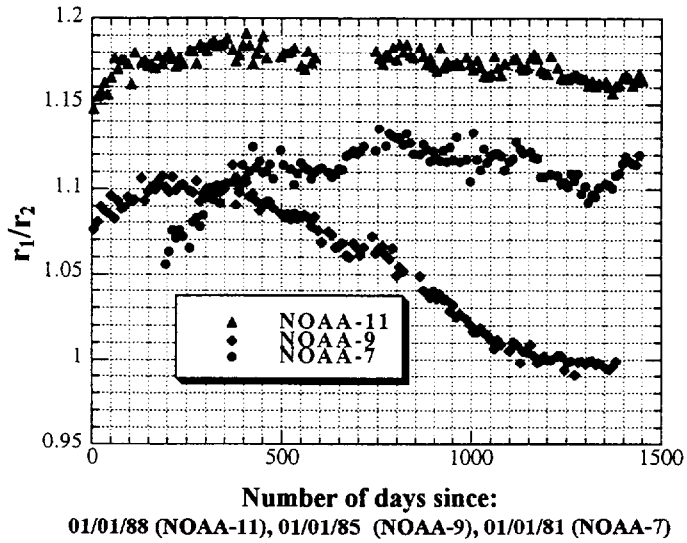

Figure 6. Ratio between the deterioration of channel 1 and 2, as observed over high reflective clouds for NOAA-7-9 and -11, as a function of the number of days since the beginning of launch year.

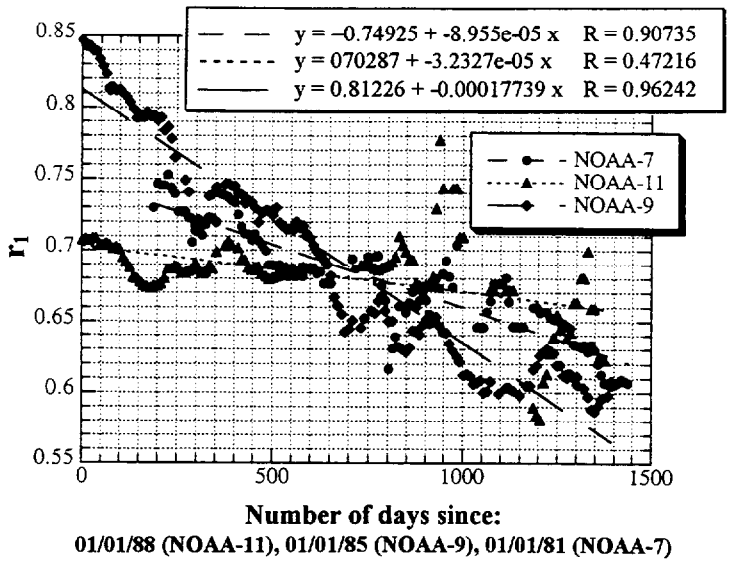

Figure 7. Deterioration of channel 1 of the AVHRR as observed using an ocean target and the method described in 3.2 for NOAA-7-9 and -11.

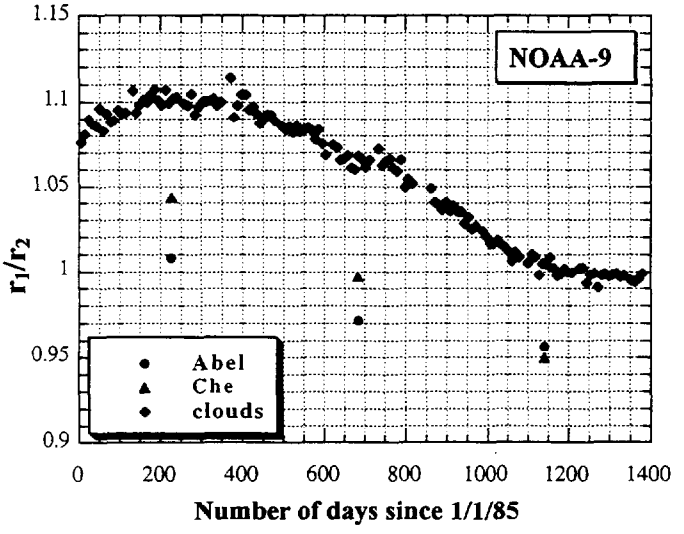

Figure 8a. Comparison of the r_1/r_2 derived using clouds and other methods for NOAA-9.

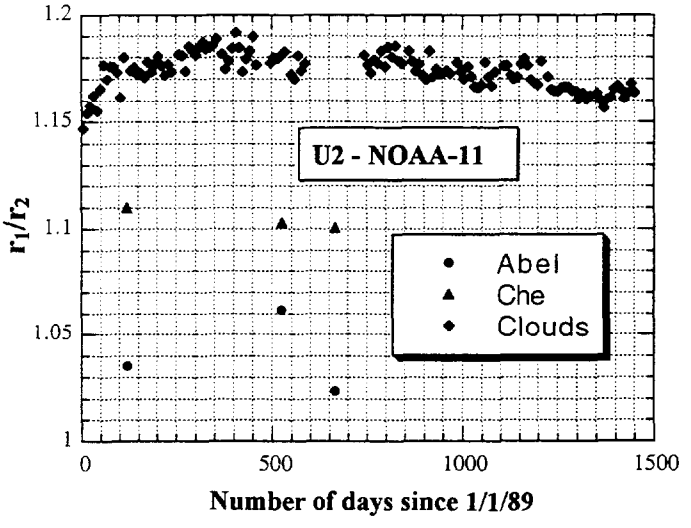

Figure 8b. Comparison of the r_1/r_2 derived using clouds and other methods for NOAA-11.

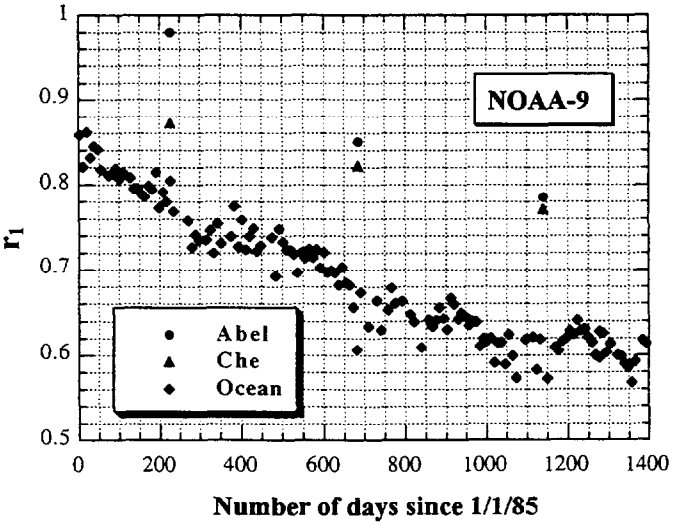

Figure 9a. Comparison of the r_1 derived using ocean and other methods for NOAA-9.

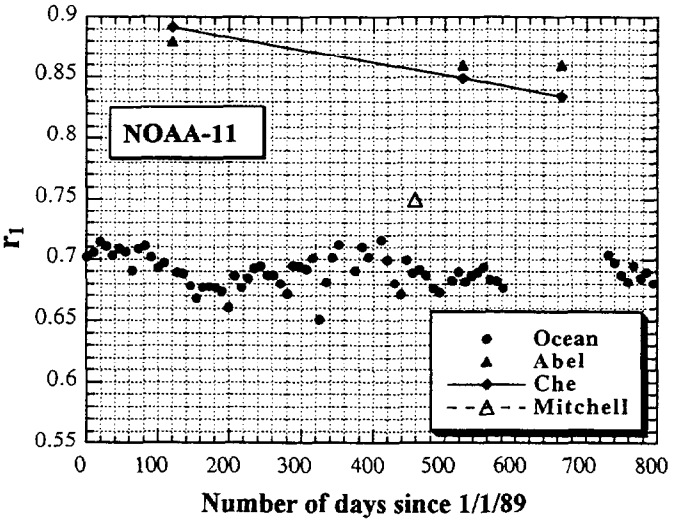

Figure 9b. Comparison of the r_1 derived using ocean and other methods for NOAA-11.

To try and explain this apparent degradation, we analysed data recorded by NOAA-9 over the coast of Tasmania where we had measurements of the optical thickness. Using the U2 absolute calibration, we derived optical thickness over the ocean in both AVHRR channels, and compared these with the actual measurements. Table 1 shows the derived values. The agreement is reasonable in channel 2 but underestimated in channel 1. Because we are in relatively good agreement with U2 concerning the ratio between the two channels, we put the result down to a problem in channel 1. Our hypothesis is that there has been a spectral shift in the response of Channel 1 to a slightly longer wavelength. Our results suggest a shift in the order of 17 nm. Such a shift due to the outgassing of the filter is reasonable as shown by Dinguirard (*personal communication*) for the SPOT-HRV instrument.

Table 1. Analysis of the optical depth values recorded over the coast of Tasmania during 1988 with those derived from NOAA-9 using calibration hypothesis.
(1) U2 calibration.
(2) U2 Calibration with a shift of 17 nm toward the red of channel 1 central wavelength.

Julian Day	τ 0.5 µm	τ 0.86 µm	τ ch1 (1) $r_1 = 0.78$	τ ch2 (1) $r_1 = 0.82$	τ ch1 (2) $r_1 = 0.78$
19	0.04	0.04	0.00	0.05	0.05
28	0.02	0.03	-0.01	0.03	0.04
31	0.10	0.09	0.06	0.12	0.10
40	0.07	0.07	-0.02	0.03	0.02
46	0.055	0.055	0.02	0.06	0.06
47	0.02	0.02	-0.03	0.02	0.02
48	0.03	0.03	-0.05	0.03	0.01
55	0.03	0.03	-0.03	0.02	0.02
57	0.06	0.06	0.05	0.11	0.11
58	0.04	0.04	0.03	0.11	0.08
65	0.03	0.03	0.01	0.06	0.06
66	0.035	0.04	-0.03	0.04	0.02
76	0.05	0.05	0.02	0.08	0.08
77	0.05	0.05	0.03	0.06	0.07
Mean	0.042	0.045	0.005	0.059	0.053

Figures 10a-b, show the results using the hypothesis of a 17 nm spectral shift in channel 1, for both NOAA-9 and 11. According to these results, this hypothesis seems reasonable for both AVHRRs. This is far from unexpected as both have similar filters and both are submitted to the same conditions during post-launch.

6. Conclusions

A new method for absolute calibration of channel 1 and 2 of AVHRR has been presented here. It consists of observations in these channels of thick high clouds and clear ocean areas. Because the clouds observed are thick and high, water vapour and gaseous absorption can be ignored, and lambertian reflectance can also be reliably assumed. Error sources are further minimised by restricting cloud observations to angles of view of between 0 and 10 degrees, and by utilising an intercalibration coefficient between channels 1 and 2, which reduces the uncertainty due to variability in surface and atmospheric conditions.

The results of the method compare well with previously published methods such as those of the Holben *et al.* (1990) desert calibration method. The ocean-cloud method we propose has the advantage that no additional measurements are necessary (although some ancillary data may be necessary to avoid areas of high and variable stratospheric aerosol content). The results overall are stable and within an acceptable error budget, yet the new approach can be used to determine sensor deterioration on a more frequent basis than other methods.

However, there are still some questions that need to be answered before the absolute calibration of AVHRR channel 1 and 2 data is completely satisfactory. Most pressing perhaps is the question concerning the possible spectral shift in channel 1. We are currently working on a combined approach based on sensor intercomparison with Peter Abel (*personal communication*) to address this point. On the other hand, the sensitivity of the Ocean method to apparent spectral shift could be seen as an advantage for characterising the calibration of ocean colour sensors such as the soon to be launched SeaWIFS.

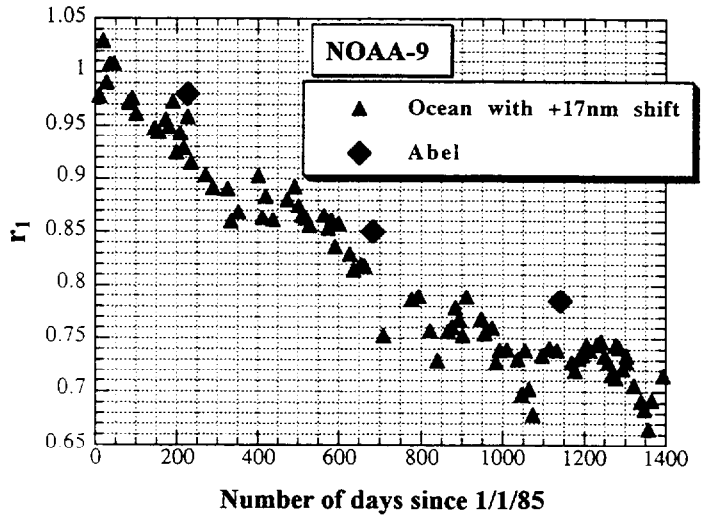

Figure 10a Comparison of the r_1 derived using ocean and other methods for NOAA-9, assuming a shift of 17 nm of the central wavelength of channel 1 toward the red.

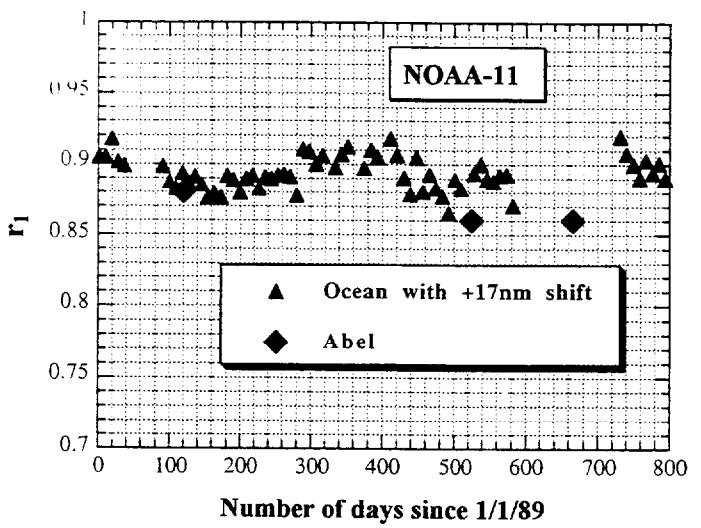

Figure 10b. Comparison of the r_1 derived using ocean and other methods for NOAA-11, assuming a shift of 17 nm of the central wavelength of channel 1 toward the red.

Glossary

θ_S	Solar zenith angle
μ_S	Cosine of solar zenith angle
θ_V	View zenith angle
μ_S	Cosine of view zenith angle
ϕ_S	Solar azimuth angle
ϕ_V	View azimuth angle
ρ	Reflectance (unitless)
Tg	Gaseous transmission
T	Total scattering transmission (diffuse+direct)
τ	Optical thickness (unitless)
s	Spherical albedo
z_t	Altitude of the target
μm	Micrometer

References and Bibliography

Abel, P., Guenther, B., Galimore, R. N. and Cooper, J. W., 1993, Calibration Results for NOAA-11 AVHRR Channels 1 and 2 from Congruent Path Aircraft observations. *Journal of Atmospheric and Oceanic Technology,* **10,** 4, 493-508.

Abramowitz, M. and Stegun, I, A., 1970, *Handbook of Mathematical Functions* (New-York: Dover Publications,Inc).

Ahmad, Z. and Fraser, R. S., 1982, An iterative radiative transfer code for ocean-atmosphere system, *Journal of Atmospheric Science,* **39,** 656-665.

Brest, C. L. and Rossow, W. L., 1991, Radiometric calibration and monitoring of NOAA AVHRR data for ISCCP. *International Journal of Remote Sensing,* **13,** 235-273.

Chandrasekhar, S., 1960, *Radiative Transfer* (Dover: New York).

Che, N. and Price, J. C., 1992, Survey of Radiometric Calibration Results and Methods for Visible and Near Infrared Channels of NOAA-7,-9, and -11 AVHRRs. *Remote Sensing of Environment,* **41,** 19-27.

Cox, C. and Munk, W., 1965, Slopes of the sea surface deduced from photographs of sun glitter. *Bulletin of Scripps Institute of Oceanography of University of California,* **6,** 401-488.

Deschamps, P. Y., Herman, M. and Tanre, D., 1983, Modeling of the atmospheric effects and its application to the remote sensing of ocean colour. *Applied Optics,* **22,** 23, 3751-3758.

Deuzé, J. L., Herman, M. and Santer, R., 1989, Fourier series expansion of the transfer equation in the atmosphere-ocean system. *Journal of Quantitative Spectroscopy and Radiative Transfer,* **41,** 6, 483-494.

Fraser, R. S. and Kaufman, Y. J., 1986, Calibration of satellite sensors after launch. *Applied Optics,* **25,** 1177-1185.

Frouin, R. and Gautier, C., 1987, Calibration of NOAA-7 AVHRR, GOES-5 and GOES-6 VISSR/VAS solar channels. *Remote Sensing Environment*, **22,** 73-101.

Holben, B. N., Kaufman, Y. J. and Kendall, J. D., 1990, NOAA-11 AVHRR visible and near-IR inflight calibration. *International Journal of Remote Sensing*, **11,** 8, 1511-1519.

Joseph, J, H., Wiscombe, W, J. and Weinman, J, A., 1976, Solar Flux Transfer Through Turbid Atmospheres EValuated by the Delta-Eddington Approximation. *Journal of Atmospheric Science*, **33,** 2452-2459.

Kaufman, Y. J. and Holben, B. N., 1993, Calibration of the AVHRR visible and near-IR bands by atmospheric scattering, ocean glint and desert reflection. *International Journal of Remote Sensing*, **14,** 21-52.

King, M., Harshvardhan D. and Arking, A., 1984, A model of the radiative properties of the El Chichon Stratospheric Aerosol layer. *Journal of Climate and Applied Meteorology*, **23,** 7, 1121-1137.

Koepke, P., 1982, Vicarious satellite calibration in the solar spectral range by means of calculated radiances and its application to Meteosat. *Applied Optics*, **21,** 15, 2845-2854.

Koepke, P., 1984, Effective reflectance of oceanic white caps. *Applied Optics*, **20,** 24,

Lenoble, J., 1977, Standard procedures to compoute Atmospheric Radiative Transfer in a Scattering Atmosphere Radiation Commission, IAMAP, National Center for Atmospheric Research, Boulder, Colorado, USA.

London, J., Bojkov, D. R., Oltmans, S. and Kelly, J. L., 1976, Atlas of the Global Distribution of the Total Ozone July 1957-June 1967 NCAR/TN/113+STR, NCAR, Boulder, Colorado, USA.

McCormick, M, P. and Veiga, R, E., 1992, SAGE II Measurements of early Pinatubo aerosols. *Geophysical Research Letters*, **19,** 2, 155-158.

Mitchell, R. M., O'Brien, D. M. and Forgan, B. W., 1992, Calibration of the NOAA AVHRR Shortwave Channels Using Split Pass Imagery: I. Pilot Study. *Remote Sensing of Environment*, **40,** 57-65.

Price, J. C., 1987, Calibration of satellite radiometers and the comparison of vegetation indexes. *Remote Sensing of Environment*, **21,** 15-27.

Price, J. C., 1988, An update on visible and near IR calibration of satellite instruments. *Remote Sensing of Environment*, **24,** 419-422.

Smith, G. R., Levin, R. H., Abel, P. and Jacobowitz, H., 1988, Calibration of the solar channels of the NOAA-9 AVHRR using high altitude aircraft measurements. *Journal of Atmospheric and Oceanic Technology*, **5,** 631-639.

Sobolev, V. V., 1975, *Light scattering in Planetry Atmospheres* , Pergamon Press, New York.

Staylor, W. F., 1990, Degradation rates of the AVHRR visible channel for the NOAA 6,7 and 9 Spacecraft. *Journal of Atmospheric and Oceanic Technology*, **7,** 411-423.

Stowe, L. L., Carey, R. M. and Pellegrino, P. P., 1992, Monitoring the Mt. Pinatubo aerosol layer with NOAA/11 AVHRR data. *Geophysical Research Letter*, **19,** 2, 159-162.

Stowe, L. L., McClain, E. P., Carey, R., Pellegrino, P., Gutman, G. G., Davis, P., Long, C. and Hart, S., 1991, Global Distribution of Cloud Cover derived from NOAA/AVHRR operational Satellite Data. *Advances in Space Research / COSPAR*, 11 COSPAR), pp. 51-54.

Tanré, D., Deroo, C., Duhaut, P., Herman, M., Morcette, J. J., Perbos, J. and Deschamps, P. Y., 1990, Description of a computer code to simulate the satellite signal in the solar spectrum: 5S code". *International Journal of Remote Sensing*, **11,** 659-668.

Tanré, D., Herman, M. and Deschamps, P. Y., 1983, Influence of the atmosphere on space measurements of directional properties. *Applied Optics*, **21,** 733-741.

Tanré, D., Holben, B. N. and Kaufman, Y. J., 1992, Atmospheric Correction algorithm for NOAA-AVHRR Products: Theory and Application. *IEEE Transaction on Geoscience and Remote Sensing*, **30,** 2, 231-248.

Teillet, P. M. and Santer, R. P., 1991, Altitude dependence in a semi-analytical atmospheric code. *Physical Measurements and Signatures in Remote Sensing, France*, ESA), pp. 36-44.

Teillet, P. M., Slater, P. N., Ding, Y., Santer, R. P., Jackson, R. D. and Moran, M. S., 1990, Three Methods for the Absolute Calibration of the NOAA AVHRR Sensors In-Flight. *Remote Sensing of Environment*, **31,** 105-120.

Vermote, E., El Saleous, N. and Holben, B, N., 1993, Atmospheric Correction of AVHRR visible and Near Infrared Data. *Workshop on Atmospheric Correction of Landsat Data*. pp. 21-25, Torrance, CA, June 29-July 1, 1993.

Vermote, E., Santer, R., Deschamps, P, Y. and Herman, M., 1991, In-flight calibration of large field of view sensors at short wavelengths using Rayleigh scattering. *International Journal of Remote Sensing*, **13,** 18, 3409-3429.

Vermote, E. F. and Tanré, D., 1992, Analytical Expressions for Radiative Properties of Planar Rayleigh Scattering Media Including Polarisation Contribution. *Preprint for Journal Of Quantitative Spectroscopy and Radiative Transfer*, **47,** 4, 305-314.

Whitlock, C. H., Staylor, W. F., Smith, G., Levin, R., Frouin, R., Gautier, C., Teillet, P. M., Slater, P. N., Kaufman, Y. J., Holben, B. N., Rossow, W. B., Brest, C. and LeCroy, S. R., 1988, AVHRR and VISSR satellite instrument calibration results for both cirrus and marine stratocumulus IFO periods. *FIRE Science Team Meeting, Vail, Colorado, USA.*

Woessner, P. and Hapke, B., 1987, Polarisation of light scattered by clover. *Remote Sensing of Environment*, **21,** 243-261.

Zdunkowski, W. G., Welch, R. M. and Korb, G., 1980, An investigation of the Structure of Typical Two-stream-methods for the Calculation of Solar Fluxes and Heating Rates in Clouds. *Contributions to Atmospheric Physics*, **53,** 2, 147-165.